Materialia 9 (2020) 100540

Contents lists available at ScienceDirect

Materialia

journal homepage: www.elsevier.com/locate/mtla

Full Length Article

Precipitation of (Ti, Zr, Nb, Ta, Hf)C high entropy carbides in a steel matrix

Wen Hao Kan[a,b,*], Yongmei Zhang[c], Xinhu Tang[d], Timothy Lucey[d], Gwénaëlle Proust[c], Yixiang Gan[c], Julie Cairney[a,b]

[a] School of Aerospace, Mechanical and Mechatronic Engineering, The University of Sydney, NSW 2006, Australia
[b] Australian Centre for Microscopy and Microanalysis, The University of Sydney, NSW 2006, Australia
[c] School of Civil Engineering, The University of Sydney, NSW 2006, Australia
[d] Weir Minerals Australia, Artarmon, NSW 2064, Australia

ARTICLE INFO

Keywords:
High entropy carbide
Metal matrix composite
Nanoindentation
Steel
Electron backscatter diffraction

ABSTRACT

In this study, arc melting was used to precipitate (Ti, Zr, Nb, Ta)C and (Ti, Zr, Nb, Ta, Hf)C particles *in-situ* within a steel matrix. Energy dispersive X-ray spectroscopy revealed that these particles are solid-solutions of their constituents (TiC, ZrC, NbC, TaC and HfC) while crystal orientation data from electron backscatter diffraction showed that the particles are either single crystals or an agglomerate of a few crystals. X-ray diffraction revealed that their lattice constants can be approximated using the rule of mixtures. The hardness of (Ti, Zr, Nb, Ta, Hf)C measured using nano-indentation was found to closely match that of TiC (the hardest and stiffest of the monocarbide constituents), indicating that the hardness is higher than what the rule of mixtures suggests. Nonetheless, better homogenization of the high entropy carbide should lead to significantly better properties. Additionally, considering the high melting points of TaC and HfC, (Ti, Zr, Nb, Ta, Hf)C may have interesting high temperature applications. Furthermore, using this approach, it should be possible to design new (Ti, Zr, Nb, Ta, Hf)C-reinforced steel matrix composites for a variety of engineering applications.

1. Introduction

In recent years, there has been growing interest in the development of multicomponent ceramics that have been termed 'high entropy', as they can exhibit higher hardness and oxidation resistance than monocarbides, and may also have potential in many high temperature applications [1,2]. A high entropy carbide is often defined as a *solid-solution* of four or five monocarbides, in near equimolar amounts, stabilized through enhanced configuration entropy which minimises the Gibb's free energy [1,3]. Alternatively, a high entropy carbide can also be defined as a carbide that has four or more principal metallic elements in near equimolar amounts or with the content of each metallic element being between 5 and 35 at% [4,5].

To date, high entropy carbides have been fabricated via a number of ways. Ye et al. showed that (Ti, Zr, Nb, Ta, Hf)C and (Ti, Zr, Nb, V)C can be synthesized using hot pressing sintering [4–6]. Similarly, Zhou et al. recently synthesized (Ti, Zr, Nb, Ta, Hf)C carbide powder using spark plasma sintering [2]. Also using the spark plasma sintering approach, Castle et al. showed that it is possible to fabricate (Ti, Zr, Ta, Hf)C and (Zr, Nb, Ta, Hf)C [1], and Harrington et al. fabricated twelve different types of high entropy carbides and found that (V, Nb, Ta, Mo, W)C showed the most promise in terms of entropic stabilization [7]. Carbothermal reduction was also shown to be a viable approach by Feng et al. [3] and Ye et al. [8] in the synthesis of (Ti, Zr, Nb, Ta, Hf)C and (Ti, Zr, Nb, Ta)C, respectively. Braic et al. demonstrated that a steel can be coated with (Ti, Zr, Nb Hf, Ta)C via magnetron sputtering [9].

With only three monocarbide components, Zhang et al. previously showed that arc melting is a viable way to fabricate (Zr, Ta, Hf)C [10]. Arc melting is a particularly interesting approach since it may be possible to precipitate (Ti, Zr, Nb, Ta, Hf)C *in-situ* within a steel matrix by simply melting the constituents of the carbide and the steel together. This is because TiC, ZrC, NbC, TaC, and HfC are carbides with a rock-salt crystal structure that are completely inter-soluble [11], and the metallic elements in these monocarbides are known to be very strong carbide formers in steel. If melted together with Fe, they will precipitate out of the melt and form a single high entropy carbide phase. Since the resulting carbide will have a rock-salt crystal structure [2], the crystal lattice resembles a high entropy face-centered cubic metallic alloy (i.e., a TiZrNbTaHf face-centered cubic alloy), but with C atoms situated at its interstitial sites. As there has been great interest in reinforcing Fe-based alloys with carbide phases such as TiC [12–15], NbC [16–19], VC [20–22], WC [23,24], and TaC [25], a steel reinforced with high entropy carbide particles may also prove to be an attractive engineering material in its own right, especially since (Ti, Zr, Nb, Ta, Hf)C have

* Corresponding author at: Australian Centre for Microscopy and Microanalysis, The University of Sydney, NSW 2006, Australia
E-mail address: wen.kan@sydney.edu.au (W.H. Kan).

https://doi.org/10.1016/j.mtla.2019.100540
Received 22 August 2019; Accepted 16 November 2019
Available online 27 November 2019

Table 1
Nominal compositions (wt%) of the steel composites fabricated with the 4C and 5C particles as were weighed out for melting. Values are balanced without including impurities.

	Ti	Zr	Nb	Ta	Hf	C	Fe
4C steel composite	3.26	6.22	6.33	12.34	–	3.28	68.57
5C steel composite	2.08	4.22	4.03	7.91	6.95	2.69	72.12

been shown to have higher hardness than its constituent monocarbides [6] and steel coatings of (Ti, Zr, Nb, Ta, Hf)C can improve wear and friction properties [9].

This study shows that it is possible to precipitate high entropy carbide particles *in-situ* within a steel matrix via arc melting. The concept was first explored using Thermo-Calc® simulations of a steel that would result in the precipitation of ($Ti_{0.25}$, $Zr_{0.25}$, $Nb_{0.25}$, $Ta_{0.25}$)C (as simulations of Hf in Fe were not available on the database used). Then, based on the results, two steel composites were fabricated, one reinforced with ($Ti_{0.23}$, $Zr_{0.27}$, $Nb_{0.25}$,$Ta_{0.25}$)C particles and the other with ($Ti_{0.18}$, $Zr_{0.21}$, $Nb_{0.20}$, $Ta_{0.21}$, $Hf_{0.19}$)C. Finally, both types of carbide phases were then characterized and benchmarked against their constituent monocarbide phases that were also fabricated using the same approach.

2. Materials and methods

2.1. Material fabrication

Thermo-Calc® simulations were undertaken to select a steel composition that was predicted to result in the precipitation of approximately 25 vol% ($Ti_{0.25}$, $Zr_{0.25}$, $Nb_{0.25}$, $Ta_{0.25}$)C particles during melting (as simulations of Hf in Fe were not available on the database used). For simplicity, we will refer to this carbide as 4C (with the number denoting the number of metallic elements). 25 vol% of carbide particles was chosen because in our previous work [26], we showed that it was possible to fabricate steels with up to 25 vol% NbC using the same arc melting system but the process became increasingly difficult at higher volume fractions.

Based on the simulation results, a composition was selected to create a sample that would precipitate 25 vol% ($Ti_{0.2}$, $Zr_{0.2}$, $Nb_{0.2}$, $Ta_{0.2}$, $Hf_{0.2}$)C, with this carbide herein referred to as 5C. For comparative purposes, a steel reinforced with 4C particles was also fabricated but with a composition that targeted a slightly higher volume fraction (30 vol%) to explore the viability of arc melting at a higher volume fraction of carbides.

Melting of the samples was done in an argon arc furnace (Edmund Bühler GmbH Arc Melter AM) with a water-chilled copper hearth and a 2% thoriated W electrode. The raw materials used for melting are Ti foil (99.7 wt% purity), Zr foil (99.92 wt% purity), Nb foil (99.8 wt% purity), Ta wire (99.95 wt% purity), Hf wire (96.7 wt% purity with 3 wt% Zr), graphite rods (99.999 wt% purity) and Fe flakes (99.95 wt% purity). The nominal compositions of both steel composites, as were weighed out, are shown in Table 1. Based on these compositions, 4C and 5C are expected to form approximately ($Ti_{0.23}$, $Zr_{0.27}$, $Nb_{0.25}$,$Ta_{0.25}$)C and ($Ti_{0.18}$, $Zr_{0.21}$, $Nb_{0.20}$, $Ta_{0.21}$, $Hf_{0.19}$)C, respectively. In order to minimize microstructural heterogeneity, the composites were flipped and re-melted five additional times. For benchmarking purposes, five steel-matrix composites, each reinforced with a single carbide type (i.e., TiC, ZrC, NbC, TaC or HfC), were also fabricated using arc melting.

2.2. Material characterization

After casting, the ingots were sectioned for microstructural characterization. All ingots were characterized by using X-ray diffraction (XRD) on a STOE STADI-P instrument equipped with a Mo source. The 4C and 5C ingots were then analysed by using electron backscatter diffraction (EBSD) and energy dispersive X-ray spectroscopy (EDS) in a Zeiss Ultra field emission gun scanning electron microscope (SEM). During EBSD acquisition (accelerating voltage 20 kV, aperture size 120 μm), the 4C and 5C carbides were indexed as the NbC phase. EDS line scans of individual particles were also conducted using a Zeiss EVO SEM with an accelerating voltage of 30 kV to generate higher energy X-ray lines. For the EDS line scan analyses, the samples were prepared by coarse grinding using SiC papers and fine polishing using 3 μm and 1 μm diamond abrasives. For EBSD, the samples were further polished using an OP-S colloidal silica suspension.

2.3. Nano-indentation tests

In order to determine the mechanical properties of the 4C and 5C carbides, as well as to compare them with their constituent monocarbides, nano-indentation tests were carried out. The nano-indentation tests were conducted using the Agilent Technologies G200 nano-indenter with a Berkovich tip. Each indentation test was conducted to a depth of 1000 nm with the surface approach distance and velocity set at 2000 nm and 10 nm/s, respectively. The target for the strain rate was set at 0.05/s. At least ten indents were conducted on the carbides for each sample to achieve statistically meaningful measurements. To calculate the elastic modulus, the Poisson's ratios of the monocarbides were specified to be 0.19 for both TiC and ZrC, 0.21 for NbC, 0.24 for TaC, and 0.18 for HfC [11]. For the 4C and 5C carbides, it was assumed that their Poisson's ratios would be the average of their constituent monocarbides, and thus, values of 0.21 and 0.20 were used, respectively. The differences in Poisson's ratios used only provided negligible variations in the calculated elastic modulus [27].

3. Results and discussion

3.1. Thermo-Calc simulations

Results from the Thermo-Calc® simulation are shown in Fig. 1. With a target volume fraction of 25%, a single 4C phase is expected to form at approximately 2700 °C (this temperature will change depending on the target volume fraction). At approximately 1469 °C, a eutectic reaction is predicted where the austenite solidifies together with approximately 3 vol% 4C. A very small amount (approximately 3 vol%) of δ-ferrite also forms in this temperature range but quickly transforms into austenite. Thermo-Calc® also predicts that at 1400 °C the 4C phase has a composition of ($Ti_{0.25}$, $Zr_{0.25}$, $Nb_{0.25}$, $Ta_{0.25}$)$C_{0.95}$, indicating some C vacancy. This suggests that, at least within this temperature range, it is likely that the proposed high entropy carbide is thermodynamically stable. Furthermore, the amount of Ti, Nb, Zr and Ta within the austenite matrix are all lower than 0.33 at%, which is consistent with the hypothesis that a high entropy carbide can form in a steel by melting a combination of carbide formers in Fe, as long as these species are insoluble in Fe. However, at a higher temperature range, the 4C composition is not equimolar in terms of its constituents. For instance, at 2500 °C, the 4C phase has a composition of ($Ti_{0.05}$, $Zr_{0.35}$, $Nb_{0.17}$, $Ta_{0.43}$)$C_{0.93}$ (with approximately 0.09 at% Fe dissolved in the carbide), indicating that ZrC and TaC, or (Zr,Ta)C, will lead the nucleation process. This is thought to be the result of differences in the solubility of the various monocarbides in liquid Fe at higher temperatures.

3.2. X-ray diffraction

The XRD results of all the fabricated ingots, including the ingots containing 30 vol% 4C and 25 vol% 5C, are shown in Fig. 2. The main phases are ferrite and the expected carbide phase. There are also some small peaks that are thought to correspond to austenite. Table 2 shows the average lattice constant calculated for each carbide from the corresponding peaks in Fig. 2, with the standard deviation for each result being less than 0.5%. Table 2 also shows the lattice constant expected

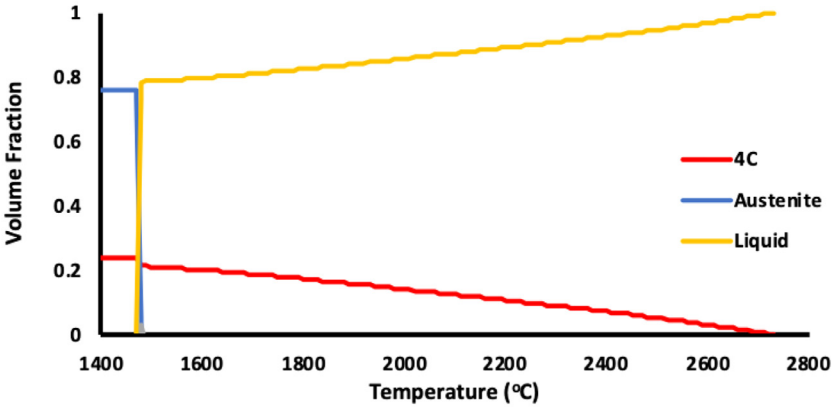

Fig. 1. Thermo-Calc® simulation of a Fe – 4C sample.

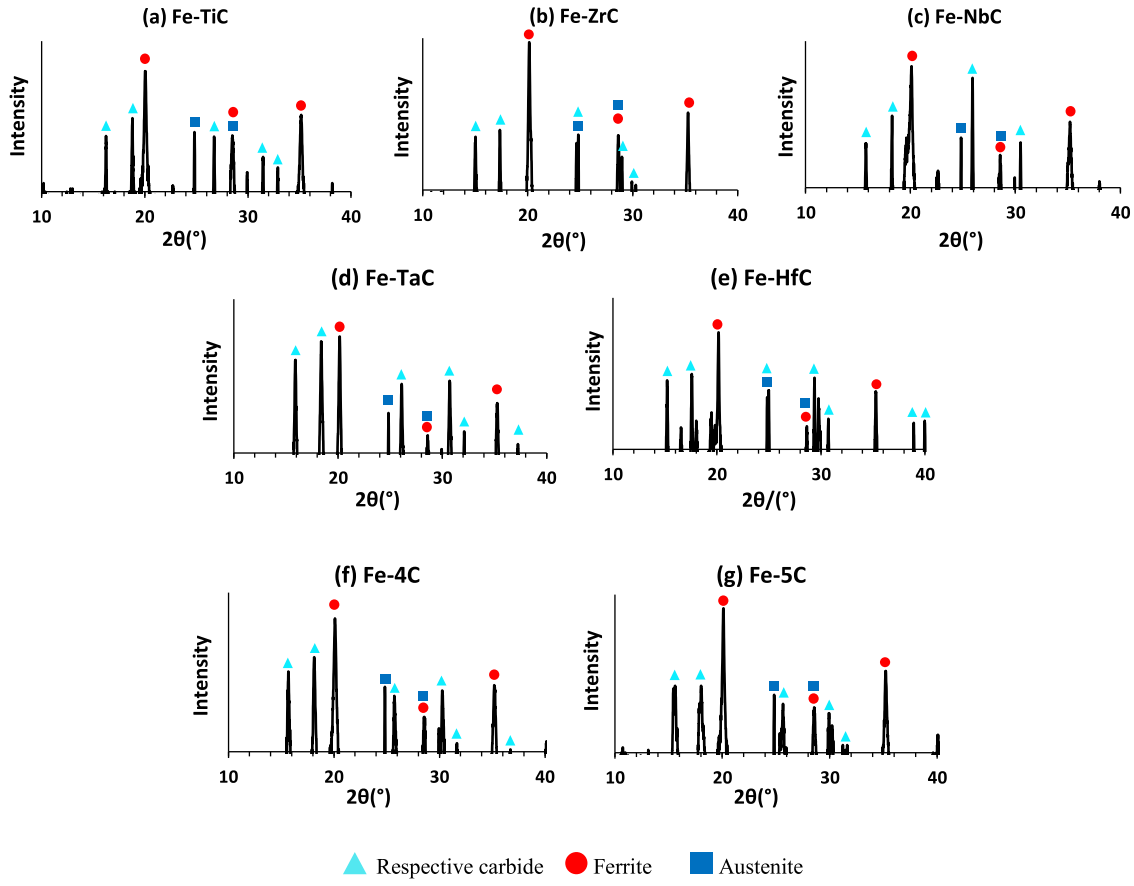

Fig. 2. XRD results of the benchmark carbides containing (a) TiC, (b) ZrC, (c) NbC, (d) TaC, and (e) HfC particles, as well as the alloys embedded with (f) 4C and (g) 5C carbide particles. The intensity axes are plotted on a logarithmic scale.

for each benchmark carbide based on the handbook by Pierson [11]. As can be observed, the calculated lattice constants for the benchmark carbides are in good agreement with the values reported by Pierson. Since two monocarbides with rock-salt crystal structures that are dissolved in one another tends to result in a lattice constant that follows the rule of mixtures [28], the lattice constants for the 4C and 5C carbides can also be predicted in the same way. By applying the rule of mixtures using the calculated lattice constants for each individual carbide reported in Table 2, and assuming the nominal carbide compositions of 4C and 5C to be $(Ti_{0.23}, Zr_{0.27}, Nb_{0.25}, Ta_{0.25})C$ and $(Ti_{0.18}, Zr_{0.21}, Nb_{0.20}, Ta_{0.21}, Hf_{0.19})C$, respectively (calculated based on the compositions reported in Table 1), the lattice constants for the 4C and 5C carbides can be predicted to be 0.4502 nm and 0.4484 nm, respectively. As shown in Table 2, the predicted lattice constant for 4C was found to be in very good agreement with the XRD result for the carbide, which was measured to be 0.4506 nm. The 5C carbide, on the other hand, was found to have a lattice parameter of 0.4529 nm (also reported in Table 2), which is higher than the 0.4484 nm predicted via the rule of mixtures.

3.3. Microstructure and composition

The microstructure of the Fe–4C ingot is shown in Fig. 3. Fig. 3(a) is a backscatter electron (BSE) image that shows the morphology of the 4C carbides at the center of the ingot. The particles are generally more than 20 μm wide and most edges are faceted. Fig. 3(b) and (c) are EBSD phase and Inverse Pole Figure (IPF) maps, respectively. The former shows that

Table 2
Average lattice constants (nm) calculated from the peaks in the XRD results in Fig. 2. The standard deviation for each result is less than 0.5%.

	TiC	ZrC	NbC	TaC	HfC	4C	5C
This study	0.4352	0.4694	0.4485	0.4450	0.4651	0.4506	0.4529
Pierson [11]	0.4328	0.4698	0.4469	0.4455	0.4636	–	–

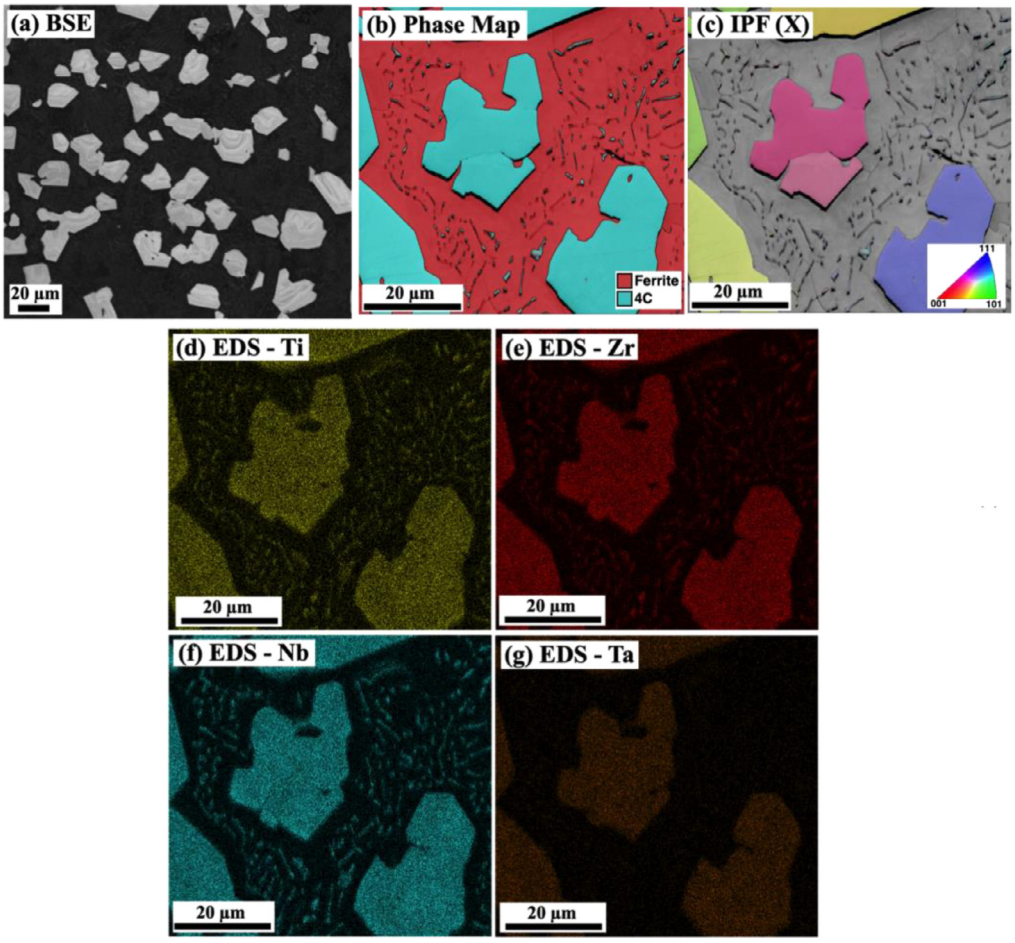

Fig. 3. Microstructure of the Fe–4C sample: (a) BSE image, (b) EBSD phase map (step-size: 0.06 µm), (c) IPF map of the 4C particles, and EDS composition maps of (d) Ti, (e) Zr, (f) Nb, and (g) Ta.

the region where the EBSD image was taken has a predominately ferrite matrix while the latter reveals that each 4C particle is either a monocrystalline particle (i.e. has a single crystal orientation) or an agglomerate of a few particles that have come into contact in the melt and bonded (i.e. two or three crystal orientations separated by a grain boundary). For instance, the particle in two shades of pink in the center of Fig. 3(c) is an agglomerate of two 4C particles. The 4C carbide appears to have also solidified as a eutectic reaction, evidenced by the highly angular needle-like structures (a morphology that is commonly referred to as a Chinese-script eutectic [29]) that are also observable between the large carbides in Fig. 3(b) and (c). Fig. 3(d)–(g) are the corresponding EDS maps of Fig. 3(b) and (c), which reveal that the 4C carbide particles have a homogeneous distribution of Ti, Zr, Nb and Ta, but the Chinese-script structures appear to be lean in Ta.

In general, the ratios of the metallic species of the 4C particles were found to range from being equi-atomic to being Ta-rich. This is illustrated in Fig. 4(a) and (b) which show EDS line scan analyses of a relatively equi-atomic particle and Ta-rich particle, respectively. These analyses exclude C, as EDS is not effective in measuring C accurately, as well as Fe, to avoid matrix interference near the edges. Excluding Fe solubility in the 4C particles, which was found to be at approximately 3 at%, the nominal compositions of the equi-atomic 4C particle and the Ta-rich 4C particle featured in Fig. 4 can be approximated as $(Ti_{0.25}, Zr_{0.25}, Nb_{0.24}, Ta_{0.26})C$ and $(Ti_{0.23}, Zr_{0.22}, Nb_{0.23}, Ta_{0.32})C$, respectively. By applying the rule of mixtures using the experimental XRD results of the constituent monocarbides, their lattice constants can be approximated to be 0.4495 nm and 0.4489 nm, respectively. While it should be noted that these results do not include the effect that 3 at% of dissolved Fe has on the lattice constant, the results are still in good agreement with the measured lattice constant of 0.4506 nm.

While the metallic species are quite homogeneously distributed in both particles that are featured in Fig. 4, there was still a slight segregation of Ta towards their cores. This segregation of Ta, as well as the lack of Ta in neighboring eutectic structures (refer to Fig. 3), suggest that TaC was the driver for 4C nucleation. Thus, the composition of a given 4C particle is tied to its precipitation history. A more Ta-rich 4C particle would have precipitated earlier from the melt as compared to a more equi-atomic 4C particle.

Overall, the experimental results are consistent with Thermo-Calc® predictions in that TaC led the precipitation but differed in that there

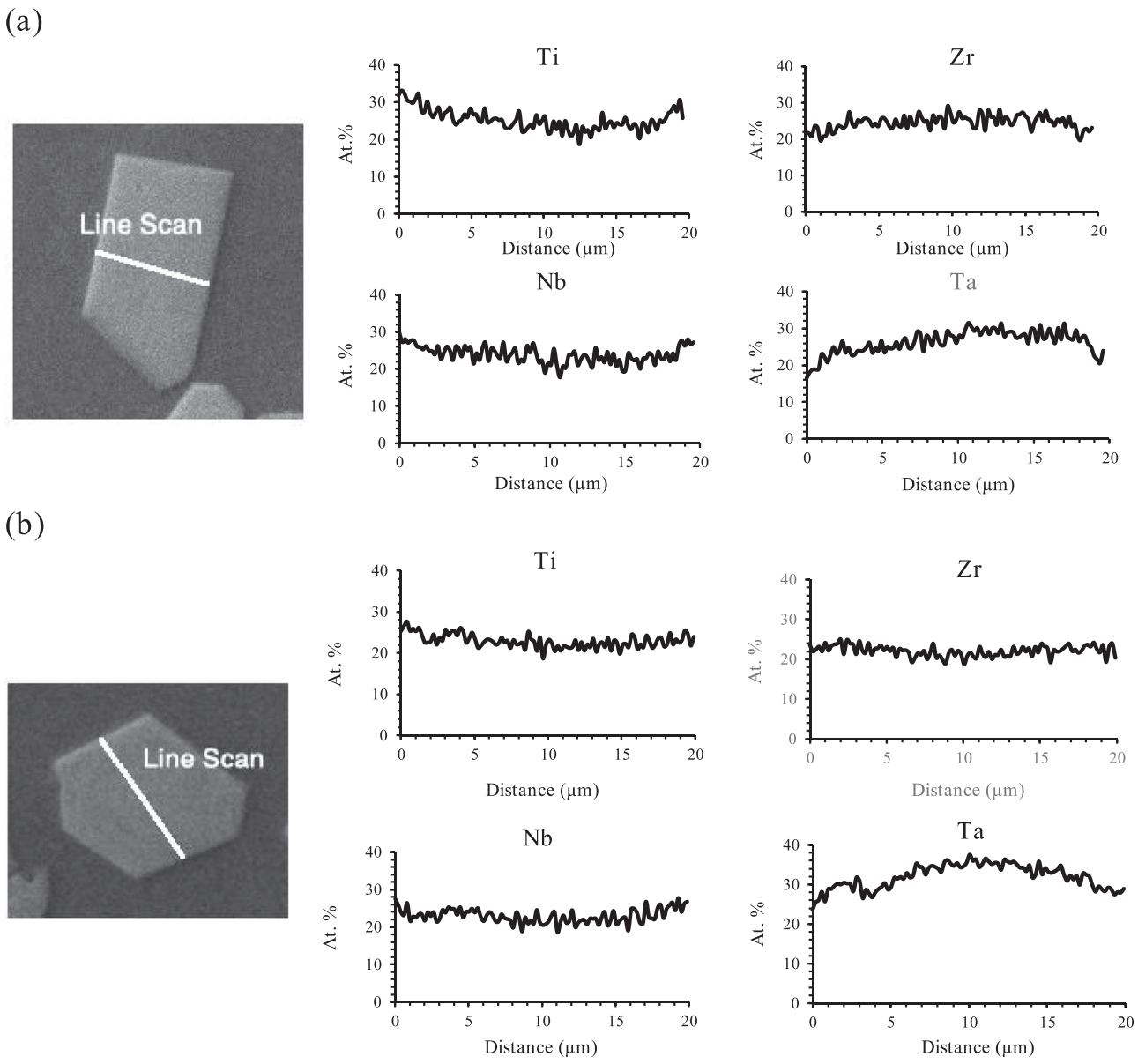

Fig. 4. EDS line scans across two 4C particles showing only the metallic species (C omitted) with the results normalized: (a) a more equi-atomic 4C particle and (b) a 4C particle that is more Ta-rich. Note that Fe solubility in the particles were found to be approximately 3 at% but was omitted to avoid matrix interference near the edges.

was no evidence that ZrC also led the precipitation. Nonetheless, the results are very promising in that the 4C particles contain a reasonable amount of all elements in solid-solution while still being relatively homogeneous.

The microstructure of the Fe–5C ingot is shown in Fig. 5. The morphology of the 5C particles is similar to those of the 4C particles in that they are also faceted (Fig. 5(a) and (b)). The 5C particles also tend to be between 10 and 50 μm wide, with each individual particle usually being a single crystal or an agglomeration of two or three crystals (as can be observed with the EBSD IPF map of the 5C particles (Fig. 5(c)). Unlike the 4C particles, however, the EDS maps (Fig. 5(d)–(h)) of the 5C particles reveal some compositional heterogeneity. In this case, the cores of the 5C carbide particles are richer in Ta and Hf, while the outer regions are richer in Ti and Nb. The Chinese-script eutectic structures, which show up more clearly in the EDS maps, are also rich in Ti, Nb, contain some Zr, and are lean in Ta and Hf. The results indicate that (Hf,Ta)C led the nucleation and precipitation of the 5C particles while partitioning NbC and TiC, and to a lesser degree, ZrC, into the melt. Therefore, once the melt was cooled to the eutectic temperature, the Nb, Zr and Ti (as well as the corresponding amount of C) atoms that had partitioned into the melt led the eutectic reaction, resulting in Chinese-script structures that are rich in Nb, Zr and Ti.

EDS line analyses conducted on the 5C particles confirm there is more compositional heterogeneity as compared to the 4C particles. It was found that Ti had the greatest propensity to be segregated towards the outer peripheries of the 5C particles, followed by Nb, while Hf and Ta were always found to be segregated toward the cores. Zr, on the other hand, was often found to have a generally linear distribution across a given 5C particle, at least with respect to the other four metals. Unlike with the 4C particles, the heterogeneous distribution of the metallic species in the 5C particles is much more distinct, resulting in a clear core-shell structure. Fig. 6 shows a 5C particle that is, on average, close to the expected nominal composition of 5C excluding Fe solubility (measured at approximately 2.8 at%). This particle has an approximate average composition of $(Ti_{0.17}, Zr_{0.22}, Nb_{0.20}, Ta_{0.24}, Hf_{0.17})C$. As can be observed, the amount of Ti and Nb at a given point is generally in-

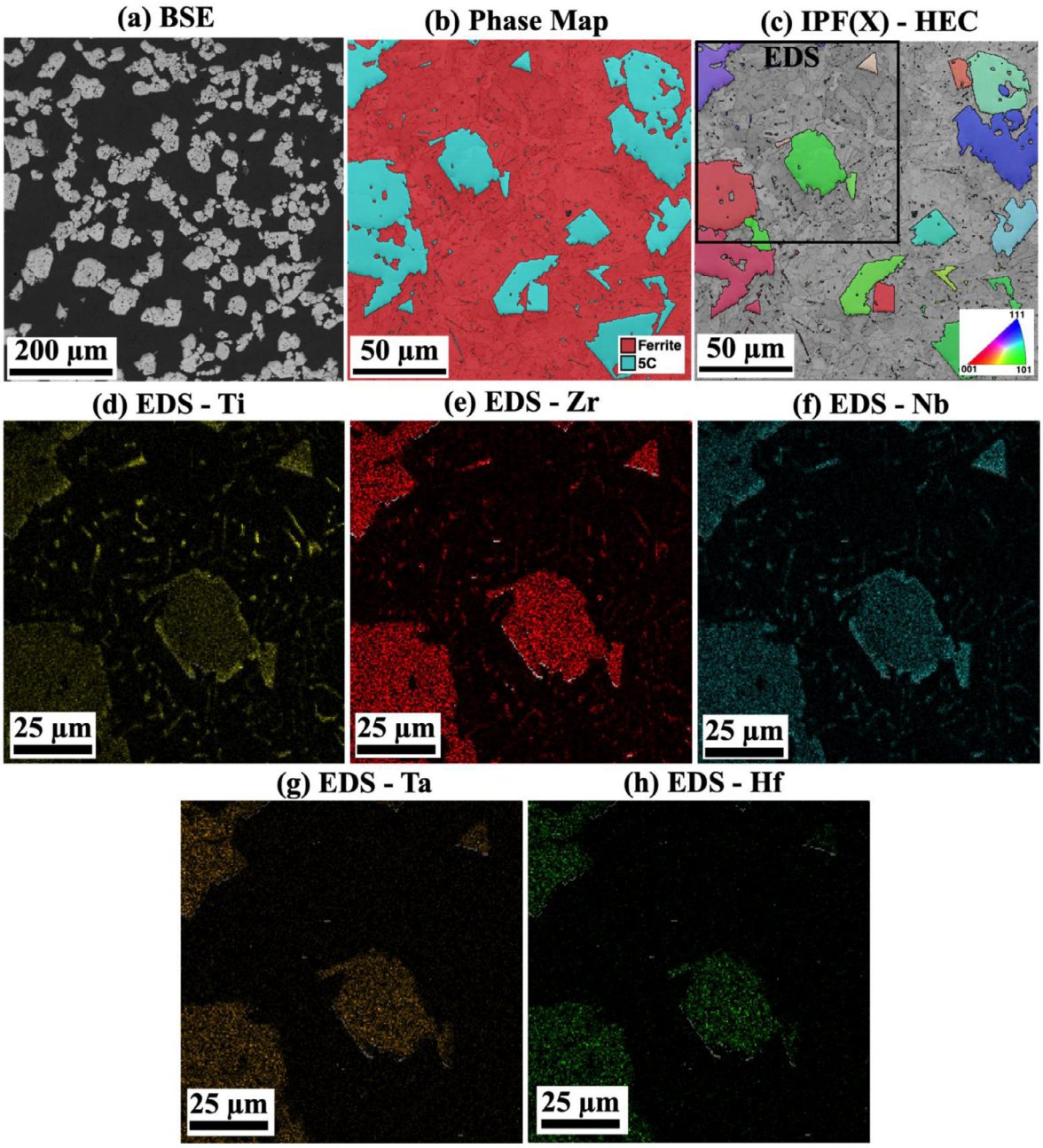

Fig. 5. Microstructure of the Fe–5C sample: (a) BSE image, (b) EBSD phase map (step-size: 0.5 µm), (c) IPF map of the 5C particles, and EDS composition maps of the region marked in (c), (d) Ti, (e) Zr, (f) Nb, (g) Ta and (h) Hf.

versely proportional to the amount of Ta and Hf. The segregation of Ti to the outer periphery is much more pronounced than that of Nb with the shell containing as much as 30 at% Ti and the core as little as 12 at% Ti. Nb, on the other hand, ranges from 28 at% at the shell to 16 at% at the core.

If it is assumed that the XRD readings of the 5C originate mainly from the primary particles, and not from the significantly finer eutectic structures (which as shown in Fig. 5, contain Ti, Zr and Nb but not Hf or Ta), the lattice constant reported in Table 2 for the 5C particles can be assumed to have mainly originated from the cores of the primary 5C particles. Since TiC has the shortest lattice constant, and most of the primary 5C particles are TiC-poor (as Ti is often segregated into the outer periphery and into the eutectic structures), it makes sense that the measured lattice constant (0.4529 nm) is much higher than the predicted lattice constant (0.4484 nm) using the rule of mixtures on the nominal composition of the melt. For instance, if the core of the 5C particle shown in Fig. 6 is defined to be the region between 4 µm and 14 µm of the line scan, its resulting composition is approximated to be ($Ti_{0.148}$, $Zr_{0.233}$, $Nb_{0.183}$, $Ta_{0.254}$, $Hf_{0.182}$)C, which results in a lattice constant of 0.4535 nm if calculated using the rule of mixtures. This is in good agreement with the measured lattice constant of 0.4529 nm.

3.4. Mechanical properties

Fig. 7(a) shows that nano-indentation to a depth of 1000 nm typically does not result in the fracturing of the carbides and the resulting indents can easily fit within individual carbide particles. The typical load-displacement curves obtained for the benchmark carbides and the high entropy carbides are shown in Fig. 7(b) and (c), respectively. Based on these results, the calculated average hardness and elastic modulus

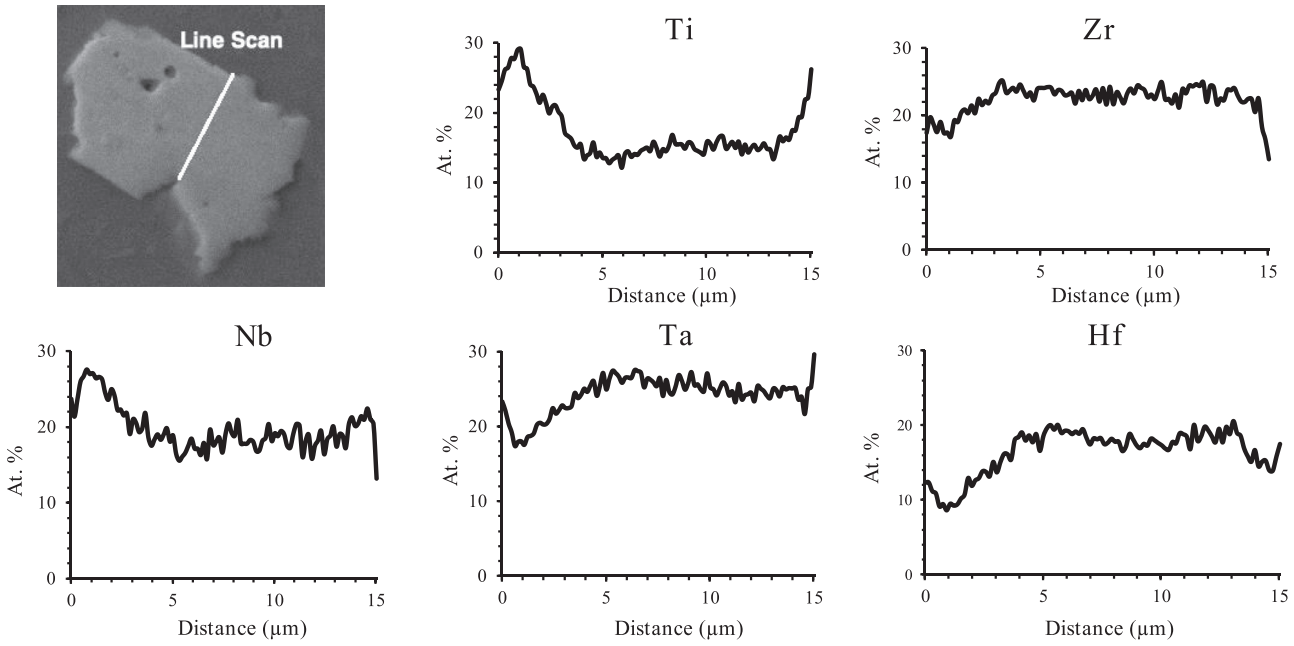

Fig. 6. EDS line scans across a 5C particle showing only the metallic species (C omitted) with the results normalized. Fe solubility in the particles were found to be approximately 2.8 at% but was omitted to avoid matrix interference near the edges.

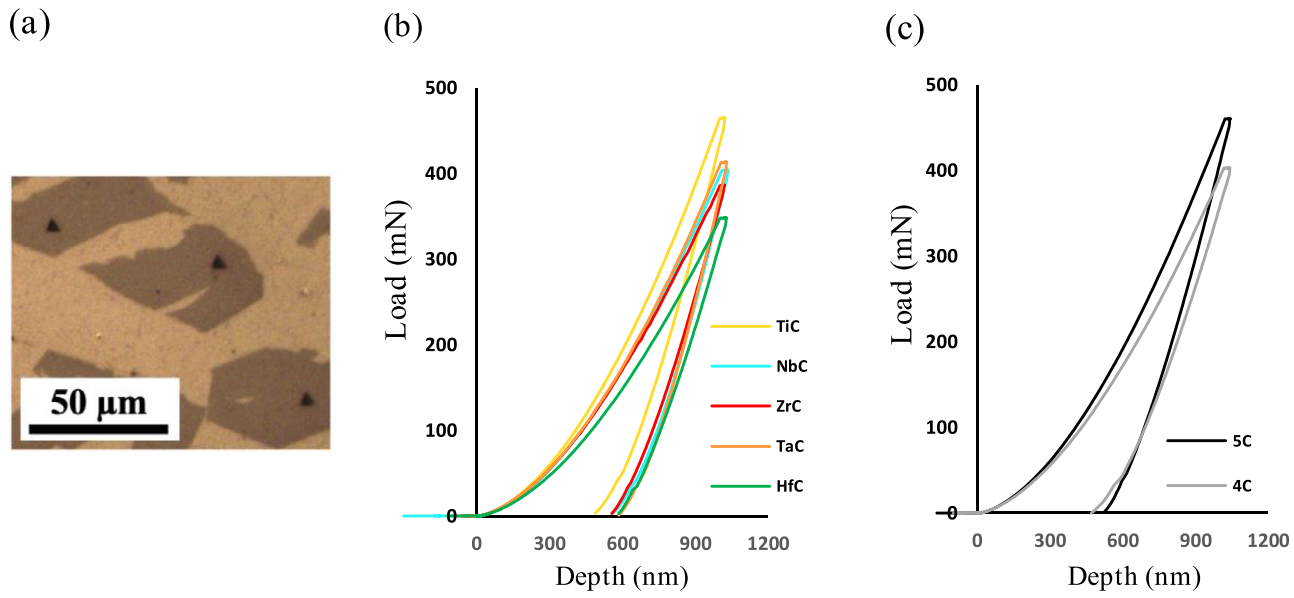

Fig. 7. Nano-indentation results of the carbides with (a) an optical microscope image showing the indents on the 5C carbides after nano-indentation to a depth of 1000 nm, and the typical load displacement curves obtained for the (b) benchmark carbides and (c) the high entropy carbides.

values at an indentation depth of 1000 nm are shown in Table 3 for each carbide type. Of the benchmark carbides, TiC typically required the highest amount of load to achieve an indentation depth of 1000 nm and has the highest elastic modulus and hardness at 412 ± 25 GPa and 33.4 ± 2.6 GPa, respectively. Conversely, with an elastic modulus of 312 ± 18 GPa, a hardness value of 24.4 ± 1.1 GPa, and the lowest load required to achieve an indentation depth of 1000 nm, HfC was the worst performer among the benchmark carbides. The mechanical properties of ZrC, NbC and TaC are in between those of TiC and HfC, and these three carbides have very similar mechanical properties.

As is also shown in Table 3, the 4C carbide has a hardness value of 27.9 GPa which is essentially the same as ZrC, NbC and TaC. However, with a value of 310 GPa, the elastic modulus of the 4C carbides is lower than all of its monocarbide constituents. The mechanical properties of 5C, on the other hand, are more interesting. Compared to 4C, 5C contains an additional monocarbide, HfC, in solid-solution. Since HfC is the worst performer in the mechanical tests relative to the other four monocarbide benchmarks, it would be reasonable to assume that 5C should perform worse than 4C. On the contrary, its hardness and elastic modulus are 14% and 23% higher than those of 4C. In fact, the mechanical properties of 5C are very similar (within error) to those of TiC.

Since 5C contains a substantial amount of TaC and HfC in solid-solution, both of which have a melting temperature that is approximately 1000 °C above TiC [11], we can expect 5C to have a much higher melting point than TiC while being able to match its mechanical properties. This may have implications for high temperature applications. Furthermore, the segregation of TiC towards the outer periph-

Table 3
Summary of the mechanical test results. The hardness and modulus results listed are obtained from an indentation depth of 1000 nm.

Carbide	Hardness (GPa)	Elastic Modulus (GPa)
TiC	33.4 ± 2.6	412.1 ± 24.8
ZrC	27.6 ± 1.9	359.0 ± 24.1
NbC	27.1 ± 2.1	389.0 ± 16.2
TaC	27.4 ± 1.9	400.5 ± 20.5
HfC	24.4 ± 1.1	312.1 ± 17.6
4C	27.9 ± 2.4	309.5 ± 17.8
5C	31.9 ± 3.1	379.2 ± 25.9

ery of the 5C particles during the fabrication process should not also be overlooked. Since TiC is the best performer in terms of mechanical properties, each 5C carbide particle is essentially be a functionally graded material with a significantly harder shell. Nonetheless, it should also be noted that at 31.9 ± 3.1 GPa, the hardness of the 5C particles is still in line with literature as values of 27.5 GPa [9], 29 GPa [7] and 40.6 GPa [6] have been reported for this type of carbide. This is despite the fact that the cores of the 5C particles are Ti-poor. In fact, if we consider the rule of mixtures on the composition of the 5C particle core shown in Fig. 6 (i.e., ($Ti_{0.148}$, $Zr_{0.233}$, $Nb_{0.183}$, $Ta_{0.254}$, $Hf_{0.182}$)C) using the monocarbide values in Table 3, the 5C particle should have a hardness and modulus of 27.7 GPa and 376 GPa, respectively. Thus, the 5C particles are within expectations for modulus but have a hardness that is 15% higher. If better homogenization can be achieved, the 5C particles should be able to approach a hardness of 40 GPa and outperform any of its constituent monocarbides, including TiC.

Assuming that better homogenization can indeed be achieved, the fact that high entropy carbides can be precipitated *in-situ* within a steel melt has implications for new steel matrix composite design. While high entropy carbides can be fabricated separately using a number of aforementioned techniques, and then used to reinforce a steel matrix, issues with wettability and interfacial reactions can occur in such *ex-situ* processes. In contrast, an *in-situ* process often results in clean interfaces between the carbides and the matrix resulting in stronger interfacial bonds [30]. Since TiC, ZrC, NbC, TaC and HfC are all very strong carbide formers in steels, the *in-situ* precipitation of 5C is not expected to significantly affect alloying elements such as Cr and Ni in the host steel matrix [19]. This means that a wide variety of steel grades can be reinforced with *in-situ* 5C particles via melting without a significant detriment to the inherent properties of the steel matrix.

Therefore, just as with conventional steel matrix composite design where reinforcing a steel with monocarbide particles can improve its hardness, wear resistance and/or strength (often at the expense of ductility and toughness) [12,13,22], reinforcing a steel with 5C particles can result in superior mechanical properties, especially if better homogenization can be achieved. Naturally, the ferrous matrix itself must also be designed with specific applications in mind. For instance, if wear performance is desired, a hard martensitic matrix [18] or a work-hardening austenitic matrix [14,23] can be considered while if corrosion resistance is required, a stainless steel matrix is ideal [17,18]. Likewise, for high temperature structural applications, a suitable stainless steel matrix can be used [15]. Excellent tensile properties, in particular, also requires that there is adequate and coherent interfacial bonding between the ferrous matrix and the ceramic reinforcing particles [13,22], which as mentioned earlier, is an added benefit of an *in-situ* manufacturing process versus an *ex-situ* one. Lastly, by etching away the ferrous matrix, this may offer an alternative fabrication method for high entropy carbide powder.

4. Conclusions

This study has demonstrated that it is possible to precipitate high entropy carbides, specifically (Ti, Zr, Nb, Ta, Hf)C particles, within a host steel matrix. The resulting high entropy carbide was found to have mechanical properties that match that of TiC, which has the best mechanical performance of the mono-carbide constituents. Since this high entropy carbide contains a substantial amount of TaC and HfC, it is also expected to have a much higher melting point than TiC, which may be useful for high temperature applications. The proposed fabrication approach has two potential applications. The first is that this approach offers an alternative manufacturing process for high entropy carbide powders by simply leeching away the steel matrix. The second is that the fabricated material is essentially steel matrix composite that is reinforced with a high entropy carbide phase, and therefore, it is, in itself, already a viable engineering material.

Declaration of Competing Interest

None.

Acknowledgments

This work was supported by the Australian Research Council [ARC Linkage Project LP130100111 – Wear-resistant alloys for the mining industry] in collaboration with Weir Minerals Australia Ltd. and The University of Sydney. The authors would also wish to acknowledge the various technical help provided by the Sydney node of Microscopy Australia (formerly known as the Australian Microscopy and Microanalysis Research Facility) at the University of Sydney.

References

[1] E. Castle, T. Csanádi, S. Grasso, J. Dusza, M. Reece, Processing and properties of high-entropy ultra-high temperature carbides, Sci. Rep. 8 (1) (2018) 8609.
[2] J. Zhou, J. Zhang, F. Zhang, B. Niu, L. Lei, W. Wang, High-entropy carbide: a novel class of multicomponent ceramics, Ceram. Int. 44 (17) (2018) 22014–22018.
[3] L. Feng, W.G. Fahrenholtz, G.E. Hilmas, Y. Zhou, Synthesis of single-phase high-entropy carbide powders, Scr. Mater. 162 (2019) 90–93.
[4] B. Ye, T. Wen, M.C. Nguyen, L. Hao, C.-Z. Wang, Y. Chu, First-principles study, fabrication and characterization of (Zr0.25Nb0.25Ti0.25V0.25)C high-entropy ceramics, Acta Mater 170 (2019) 15–23.
[5] B. Ye, T. Wen, D. Liu, Y. Chu, Oxidation behavior of ($Hf_{0.2}Zr_{0.2}Ta_{0.2}Nb_{0.2}Ti_{0.2}$)C high-entropy ceramics at 1073–1473K in air, Corros. Sci. 153 (2019) 327–332.
[6] B. Ye, T. Wen, K. Huang, C.Z. Wang, Y. Chu, First-principles study, fabrication, and characterization of ($Hf_{0.2}Zr_{0.2}Ta_{0.2}Nb_{0.2}Ti_{0.2}$) C high-entropy ceramic, J. Am. Ceram. Soc. 102 (7) (2019) 4344–4352.
[7] T.J. Harrington, J. Gild, P. Sarker, C. Toher, C.M. Rost, O.F. Dippo, C. McElfresh, K. Kaufmann, E. Marin, L. Borowski, P.E. Hopkins, J. Luo, S. Curtarolo, D.W. Brenner, K.S. Vecchio, Phase stability and mechanical properties of novel high entropy transition metal carbides, Acta Mater. 166 (2019) 271–280.
[8] B. Ye, S. Ning, D. Liu, T. Wen, Y. Chu, One-step synthesis of coral-like high-entropy metal carbide powders, J. Am. Ceram. Soc. (2019).
[9] V. Braic, A. Vladescu, M. Balaceanu, C.R. Luculescu, M. Braic, Nanostructured multi-element (TiZrNbHfTa)N and (TiZrNbHfTa)C hard coatings, Surf. Coat. Technol. 211 (2012) 117–121.
[10] Z. Zhang, S. Fu, F. Aversano, M. Bortolotti, H. Zhang, C. Hu, S. Grasso, Arc melting: a novel method to prepare homogeneous solid solutions of transition metal carbides (Zr, Ta, Hf), Ceram. Int. 45 (7, Part A) (2019) 9316–9319.
[11] H.O. Pierson, Handbook of Refractory Carbides and Nitrides: Properties, Characteristics, Processing and Apps, William Andrew, 1996.
[12] Z. Wang, T. Lin, X. He, H. Shao, B. Tang, X. Qu, Fabrication and properties of theTiC reinforced high-strength steel matrix composite, Int. J. Refract. Metals Hard Mater. 58 (2016) 14–21.
[13] N.R. Oh, S.K. Lee, K.C. Hwang, H.U. Hong, Characterization of microstructure and tensile fracture behavior in a novel infiltrated TiC–steel composite, Scr. Mater. 112 (2016) 123–127.
[14] A.K. Srivastava, K. Das, The abrasive wear resistance of TiC and (Ti,W)C-reinforced Fe–17Mn austenitic steel matrix composites, Tribol. Int. 43 (5) (2010) 944–950.
[15] Y.-H. Lee, S. Ko, H. Park, D. Lee, S. Shin, I. Jo, S.-B. Lee, S.-K. Lee, Y. Kim, S. Cho, Effect of TiC particle size on high temperature oxidation behavior of TiC reinforced stainless steel, Appl. Surf. Sci. 480 (2019) 951–955.
[16] W. Zapata, C. Da Costa, J. Torralba, Wear and thermal behaviour of M2 high-speed steel reinforced with NbC composite, J. Mater. Sci. 33 (12) (1998) 3219–3225.
[17] K.-T. Huang, S.-H. Chang, P.-C. Hsieh, Microstructure, mechanical properties and corrosion behavior of NbC modified AISI 440C stainless steel by vacuum sintering and heat treatments, J. Alloys Compd. 712 (2017) 760–767.

[18] W.H. Kan, G. Proust, V. Bhatia, L. Chang, K. Dolman, T. Lucey, X. Tang, J. Cairney, Slurry erosion, sliding wear and corrosion behavior of martensitic stainless steel composites reinforced in-situ with NbC particles, Wear 420 (2019) 149–162.
[19] W.H. Kan, V. Bhatia, K. Dolman, T. Lucey, X. Tang, L. Chang, G. Proust, J. Cairney, A study on novel AISI 304 stainless steel matrix composites reinforced with (Nb0. 75, Ti0. 25) C, Wear 398 (2018) 220–226.
[20] Z. Zhang, T. Yu, R. Kovacevic, Erosion and corrosion resistance of laser cladded AISI 420 stainless steel reinforced with VC, Appl. Surf. Sci. 410 (2017) 225–240.
[21] Y. Wang, Y. Ding, J. Wang, F. Cheng, J. Shi, In situ production of vanadium carbide particulates reinforced iron matrix surface composite by cast-sintering, Mater. Des. 28 (7) (2007) 2202–2206.
[22] E.G. Moghaddam, N. Karimzadeh, N. Varahram, P. Davami, Impact–abrasion wear characteristics of in-situ VC-reinforced austenitic steel matrix composite, Mater. Sci. Eng.: A 585 (2013) 422–429.
[23] G.-S. Zhang, J.-D. Xing, Y.-M. Gao, Impact wear resistance of WC/Hadfield steel composite and its interfacial characteristics, Wear 260 (7–8) (2006) 728–734.
[24] R. Zhou, Y. Jiang, D. Lu, The effect of volume fraction of WC particles on erosion resistance of WC reinforced iron matrix surface composites, Wear 255 (1–6) (2003) 134–138.
[25] N. Zhao, Y. Xu, L. Zhong, Y. Yan, K. Song, L. Shen, V.E. Ovcharenko, Fabrication, microstructure and abrasive wear characteristics of an in situ tantalum carbide ceramic gradient composite, Ceram. Int. 41 (10, Part A) (2015) 12950–12957.
[26] W.H. Kan, Z.J. Ye, Y. Zhu, V.K. Bhatia, K. Dolman, T. Lucey, X. Tang, G. Proust, J. Cairney, Fabrication and characterization of microstructure of stainless steel matrix composites containing up to 25 vol% NbC, Mater. Charact. 119 (2016) 65–74.
[27] W.C. Oliver, G.M. Pharr, An improved technique for determining hardness and elastic modulus using load and displacement sensing indentation experiments, J. Mater. Res. 7 (6) (1992) 1564–1583.
[28] G. Samsonov, G.S. Upadkhaya, Properties of alloys of niobium and titanium carbides in their homogeneity region, Powder Metall. Metal Ceram. 7 (9) (1968) 723–726.
[29] F. Haddad, S.E. Amara, R. Kesri, Liquidus surface projection of the Fe–Nb–C system in the iron-rich corner, Metall. Mater. Trans. A 39 (5) (2008) 1026–1033.
[30] F. Akhtar, Microstructure evolution and wear properties of in situ synthesized TiB_2 and TiC reinforced steel matrix composites, J. Alloys Compd. 459 (1) (2008) 491–497.